

Article

Effect of the Annealing Conditions on the Strain Responses of Lead-Free $(\text{Bi}_{0.5}\text{Na}_{0.5})\text{TiO}_3\text{-BaZrO}_3$ Ferroelectric Thin Films

Zhe Wang, Jinyan Zhao * and Wei Ren *

Electronic Materials Research Laboratory, Key Laboratory of the Ministry of Education, International Center for Dielectric Research, School of Electronic Science and Engineering & International Joint Laboratory for Micro/Nano Manufacturing and Measurement Technology, Xi'an Jiaotong University, Xi'an 710049, China

* Correspondence: zhaoyj7@xjtu.edu.cn (J.Z.); wren@mail.xjtu.edu.cn (W.R.)

Abstract: Bismuth sodium titanate $(\text{Bi}_{0.5}\text{Na}_{0.5})\text{TiO}_3$ (BNT)-based thin films have attracted large attention for the production of modern precise micro-devices due to their outstanding strain responses. However, obtaining good electrical properties and low leakage current in BNT-based thin films is still a great challenge. In this work, $0.945(\text{Bi}_{0.5}\text{Na}_{0.5})\text{TiO}_3\text{-}0.055\text{BaZrO}_3$ (BNT-5.5BZ) thin films were deposited by the chemical solution deposition (CSD) method and annealed under two different conditions. This work describes a careful research study on the influence of the annealing conditions on the crystalline structure, morphology, and electrical performance of the BNT-5.5BZ thin films. The films exhibited a dense structure and excellent electrical properties following an optimized thermal treatment process. An ultra-high strain response of 1.5% with a low dielectric loss of ~ 0.03 was obtained in the BNT-5.5BZ thin films after post-annealing in an O_2 atmosphere. The results of this work show that the enhanced strain response was mainly due to a reversible field-induced phase transition between the ferroelectric phase and the relaxation state. The post-annealing treatment is an effective method to optimize the electrical properties of BNT-based films, providing many opportunities for the application of ferroelectric devices.

Keywords: lead-free thin films; post-annealing; strain response; bismuth sodium titanate



Citation: Wang, Z.; Zhao, J.; Ren, W. Effect of the Annealing Conditions on the Strain Responses of Lead-Free $(\text{Bi}_{0.5}\text{Na}_{0.5})\text{TiO}_3\text{-BaZrO}_3$ Ferroelectric Thin Films. *Crystals* **2023**, *13*, 606. <https://doi.org/10.3390/cryst13040606>

Academic Editors: Pankaj Sharma and Artem Pronin

Received: 28 February 2023

Revised: 21 March 2023

Accepted: 31 March 2023

Published: 2 April 2023



Copyright: © 2023 by the authors. Licensee MDPI, Basel, Switzerland. This article is an open access article distributed under the terms and conditions of the Creative Commons Attribution (CC BY) license (<https://creativecommons.org/licenses/by/4.0/>).

1. Introduction

With the continuous development of the green information society, the problem of environmental pollution caused by lead volatilization from commercial mainstream ferroelectric devices is becoming increasingly serious. There is a great demand for research on novel high-performance lead-free perovskite materials in the modern society [1–3]. $(\text{Bi}_{0.5}\text{Na}_{0.5})\text{TiO}_3$ (BNT), one of the typical lead-free ferroelectric materials, has received close attention due to its outstanding strain responses in applications involving high-precision actuators [4]. S.-T. Zhang et al. first reported high-strain $(\text{K}_{0.5}\text{Na}_{0.5})\text{NbO}_3$ modified BNT- BaTiO_3 (BNT-BT-KNN) with a large strain performance of 0.45% in 2007 [5]. Subsequently, X.L. Tan et al. achieved an enhanced electro-strain value of 0.70% in BNT ceramics with the substitution of Nb element (BNT-2.5Nb) on the B-site [6]. In addition, for ferroelectric thin films, important components in semiconductor technologies, it is urgent to improve electrical performance and decrease the leakage [7]. Many key issues must be seriously considered, such as large leakage and loss, complex composition control, and electrical properties enhancement [3]. Therefore, realizing BNT-based thin films with good electrical properties and decreased leakage faces many challenges.

Among many deposition technologies for thin films, chemical solution deposition (CSD) is cost-effective and suitable for preparing films with complex compositions [8–11]. The heating process for the conversion of solution-deposited uncrystallized layers into shaped thin films plays a significant effect on the crystallization and electrical performances of the films [12]. For BNT-based materials in the form of thin films, the volatility of alkali metal elements such as Na and Bi during heating limits the annealing treatment to a

lower temperature range. Compared with their ceramic counterparts, the characteristics of BNT-based films, e.g., grain size and holes on the surface and inside the films, have important impacts on the dielectric/ferroelectric properties. Therefore, realizing high-quality BNT-based films need a serious control of the experimental procedure and an effective annealing treatment. Post-annealing treatment is a common method for as-deposited thin films. After post-annealing at 700 °C for 20 min, the quality and performance of $\text{PbZr}_{0.3}\text{Ti}_{0.7}\text{O}_3$ (PZT) films were significantly improved: the surface was smoother, and both ferroelectric and pyroelectric properties were improved [13]. $(\text{K}_{0.5}\text{Na}_{0.5})\text{NbO}_3$ (KNN) thin films exhibited enhanced electrical properties and ameliorated leakage after post-annealing [14]. In addition, annealing treatments in certain atmospheres, such as O_2 and N_2 , applied to the ferroelectric materials in ceramics and thin films have also been researched [15,16]. Annealing the film at a high temperature in an O_2 atmosphere forces oxygen vacancies to appear on the film surface, filling them with oxygen, and promoting the growth of the grains [17]. The films gradually become denser, with increased grain size and grain uniformity. Improved energy storage properties of $\text{Ba}_{0.85}\text{Ca}_{0.15}\text{Ti}_{0.90}\text{Zr}_{0.10}\text{O}_3$ (BCZT) thin films were obtained by annealing in an oxygen-enriched atmosphere [18]. That is to say, annealing in an O_2 atmosphere is a useful method to optimize the quality and electrical properties of BNT-based thin films.

2. Experiments

In this work, $0.945(\text{Bi}_{0.5}\text{Na}_{0.5})\text{TiO}_3-0.055\text{BaZrO}_3$ (BNT-5.5BZ) thin films were deposited on polycrystalline Pt/ $\text{TiO}_2/\text{SiO}_2/\text{Si}$ (001) substrates through the CSD method. We chose BNT-5.5BZ ceramics on the basis of a previous systematic study of their morphotropic phase boundary (MPB) composition [19]. Two different annealing conditions were used to enhance the electrical performance for of BNT-5.5BZ thin films: (1) one-step annealing at a high temperature of 725 °C; (2) two-step method, first annealing at a lower temperature of 650 °C, then post-annealing at 725 °C in an O_2 atmosphere. This article provides a careful study on the influence of different annealing conditions on BNT-5.5BZ thin films. An optimal strain property of ~1.5% was recorded for the samples using two-step annealing.

2.1. Precursor Solution Preparation

The $0.945(\text{Bi}_{0.5}\text{Na}_{0.5})\text{TiO}_3-0.055\text{BaZrO}_3$ (BNT-5.5BZ) thin films were fabricated by the CSD method, followed by repeated spin-coating and annealing processes. The preparation of the BNT-5.5BZ precursor was carried out by using two solutions (labeled as solution I and solution II). Solution I was first prepared by dissolving $(\text{CH}_3\text{COO})_2\text{Ba}$ (barium acetate, analytically pure, Sigma-Aldrich, Munich, Germany), CH_3COONa (sodium acetate, analytically pure, Sigma-Aldrich, Munich, Germany), and $(\text{CH}_3\text{COO})_3\text{Bi}$ (bismuth acetate, 4N, Alfa-Aesar, Haverill, MA, USA), after weighing according to the stoichiometric ratio. Notably, a 10 mol% Na and a 2 mol% Bi starting materials excess was placed into solution I to compensate for their volatilization during the heating process. Then, the solvents $\text{C}_3\text{H}_8\text{O}_2$ (2-methoxyethanol, analytical pure, Sinopharm Chemical Reagent Co., Ltd., Shanghai, China) and CH_3COOH (acetic acid, analytical pure, Sinopharm Chemical Reagent Co., Ltd., Shanghai, China) were mixed into solution I, magnetically stirring for 1 h at 90 °C. Solution II was prepared by dissolving $(\text{C}_4\text{H}_9\text{O})_4\text{Ti}$ (tetrabutyl titanate, chemically pure, Sigma-Aldrich, Munich, Germany) into $\text{C}_3\text{H}_8\text{O}_2$, adding $\text{CH}_3\text{COCH}_2\text{COCH}_3$ (acetylacetone, analytically pure, Sigma-Aldrich, Munich, Germany), and continually stirring for 40 min at room temperature (RT). The addition of $\text{CH}_3\text{COCH}_2\text{COCH}_3$, as a polymerizing agent and stabilizer, prevented the hydrolysis of $(\text{C}_4\text{H}_9\text{O})_4\text{Ti}$. Then, $(\text{C}_4\text{H}_9\text{O})_4\text{Zr}$ (zirconium tetra-*n*-butoxide, 80 wt%, Sigma-Aldrich, Munich, Germany) was added to solution II, followed by continuous stirring for 20 min at RT. Finally, solution II was slowly added to solution A while mildly mixing. After stirring at RT for 1 h and static aging for more than 1 day, the final BNT-5.5BZ precursor solution was obtained.

2.2. Film Fabrication

Before the thermogravimetry (TG) and differential scanning calorimetry (DSC) measurements, the BNT–5.5BZ gel was dried at 80 °C on a hot stage. Then, TG and DSC curves were obtained for a dried BNT–5.5BZ gel powder to determine the appropriate annealing conditions, as shown in Figure 1. Three decomposition steps occurred for a total mass loss of ~55% upon heating from 40 °C to 800 °C in a N₂ atmosphere. The first step, with a mass loss of 7%, took place up to 200 °C due to the evaporation of the absorbed water. Then, a mass loss of 35% occurred near 416 °C, showing an exothermic event. It indicated that the remaining organics and other volatiles were removed around this temperature [20]. Finally, up to ~660 °C, a 13% mass loss occurred which might be due to the crystallization of the BNT–5.5BZ thin films. During the heating process of the films, the evaporation of water was proceeded at 150 °C, then at 420 °C, the removal of organics and volatiles took place, and last, >650 °C, the nucleation and crystallization of the films occurred. This process is commonly used for the preparation of BNT–based thin films [7,8].

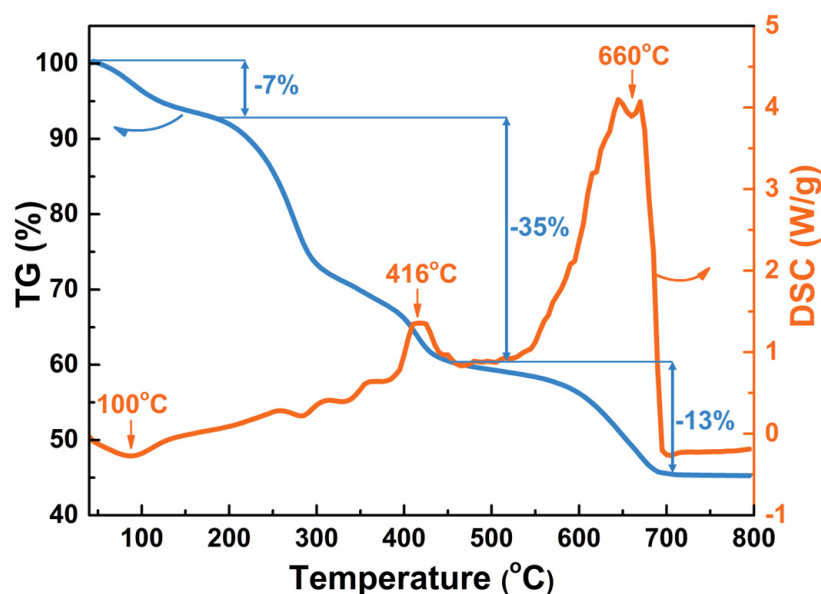


Figure 1. The TG and DSC curves of the BNT–5.5BZ dried gel powder heated from 40 °C to 800 °C. (The TG curve was shown by the blue line, and the DSC curve was marked by the orange line).

The preparation of BNT–5.5BZ thin films was divided into two steps: spin–coating and annealing. All BNT–5.5BZ thin films were deposited on polycrystalline Pt/TiO₂/SiO₂/Si (001) substrates. First, spin–coating proceeded at 3000 revolutions per minute for 40 s. A single wet gel layer was submitted to a heating process: 150 °C for 3 min and 420 °C for 10 min, using a rapid thermal process, leading to the evaporation and removal of the residual organics. Then, two annealing processes were used to form the films. One–step annealing for the single–layer film was conducted at 725 °C for 3 min for nucleation and crystallization. After repeating the spin–coating and annealing processes six times, the BNT–5.5BZ thin films were obtained with the desired thickness (the samples were labeled as “725 °C”). The two–step method for the single–layer film consisted in annealing at 650 °C for 3 min after pyrolyzing according to the TG and DSC results, then repeating the spin–coating and annealing processes for six times. Finally, the films were post–annealed at 725 °C for 30 min in an O₂ atmosphere (the samples were labeled as “650 °C + 725 °C”).

2.3. Characterizations

For exploring the weight change and thermal performance of the BNT–5.5BZ thin films, thermogravimetry (TG) and differential scanning calorimetry (DSC, STA449F5 Jupiter,

NETZSCH, Waldkraiburg, Bayern, Germany) were performed from 40 °C to 800 °C on the BNT-5.5BZ thin films in a N₂ atmosphere. The samples' average structure and local structure obtained after annealing under different conditions were used for X-ray diffraction and Raman spectrometry. The instruments used were a high-resolution X-ray diffractometer (XRD, Empyrean, PANalytical, Almelo, The Netherlands) with Cu K α 1 radiation ($\lambda = 1.5406 \text{ \AA}$) and a Raman spectrometer (LabRAM HR Evolution, Horiba, Montpellier, France) with a 532 nm laser. For the surface and cross-sectional morphologies of the BNT-5.5BZ thin films, pictures were taken by a scanning electron microscope (Gemini SEM 500, Carl Zeiss, Jena, Germany). For the electrical measurements (such as dielectric, ferroelectric, strain response, and so on), electrodes on the surface of the samples were necessary. Gold electrodes ($\varphi = 300 \text{ \mu m}$) were prepared by a direct current (DC) sputtering. The frequency and temperature dependence of dielectric constant and dielectric loss of the BNT-5.5BZ thin films were determined by a precision impedance analyzer (E4980a, Agilent Technologies Inc., Santa Clara, CA, USA). The leakage current densities under different electric fields were ensured using a semiconductor characterization system (4200-SCS, Keithley Instruments Inc., Cleveland, OH, USA). The polarization (P) and strain response as a function of the electrical fields (E) (P - E and S - E hysteresis loops) were characterized using a ferroelectric analyzer (TF analyzer 2000, aixACCT, Aachen, Germany) with a double-beam laser interferometer (aixDBLI, aixACCT, Aachen, Germany). The out-of-plane displacement-voltage hysteresis loops and phase-voltage hysteresis loops of the BNT-5.5BZ samples were obtained by a scanning force microscope (Dimension Icon, Bruker, Billerica, MA, USA) in piezoresponse force microscopy (PFM) mode with a conductive tip (DDESP, resonant frequency $\sim 450 \text{ kHz}$, spring constant = 80 N, Bruker, Billerica, MA, USA).

3. Results and Discussion

Figure 2a shows the X-ray diffraction results from 20° to 60° of the BNT-5.5BZ thin films annealed under different conditions. There are five independent diffraction peaks in this 2θ range, as shown in Figure 2a. Except for the intense Pt (111) peaks near 39.7° and the weak Au (111) peaks (top and bottom electrodes) near 37.9°, the four independent diffraction peaks correspond to (001), (110), (002), and (112) of a single phase of perovskite structure for the BNT-5.5BZ thin films. Unlike preferred oriented films, the BNT-5.5BZ thin films in this work possessed a polycrystalline structure characterized by four diffraction peaks. In addition, all the samples annealed in different conditions presented a similar single-phase structure without any secondary phase. The BNT-5.5BZ thin films were well crystallized at an annealing temperature exceeding 650 °C, following the crystallization temperature from the TG and DSC curves in Figure 1. The X-ray diffraction peaks of all BNT-5.5BZ samples in Figure 2a shifted to a lower 2θ angle, due to of Ba²⁺, Zr⁴⁺, with the large atomic radii, replacing Bi³⁺, Na⁺, and Ti⁴⁺, with small atomic radii [8], compared with those of pure BNT. Furthermore, this shift was more evident for the "650 °C + 725 °C" films, indicating that the post-annealing treatment of the BNT-5.5BZ thin films promoted the diffusion of the BZ component into the BNT lattice and enhanced the crystallization. To further study the local structure of the BNT-5.5BZ thin films, Raman spectra were collected at RT, as presented in Figure 2b-d. The spectral deconvoluted results of the BNT-5.5BZ thin films were obtained according to Gaussian-Lorentzian modes [21]. Four different fitted peaks (A_1 , A_2 , B_1 , and B_2) are shown, while the corresponding locations of the fitted peaks are marked in Figure 2b-d. Two main vibration regions are present for all BNT-5.5BZ thin films in Figure 2b-d. One (Region A) is the vibrations of the Ti-O mode in the range of 180 cm^{-1} - 400 cm^{-1} , and the other (Region B) is the vibration of the TiO₆ octahedra in the range of 450 cm^{-1} - 700 cm^{-1} [22,23]. In Region A, the locations of the fitted A_1 and A_2 peaks shift simultaneously to lower frequencies as shown in Figure 2b-d, while the fitted B_1 and B_2 peaks in Region B shift simultaneously to higher frequencies, indicating that the post-annealing treatment played a noticeable effect on the local structure of the BNT-5.5BZ thin films. In our previous work, the Raman fitted results exhibited a similar

tendency as the XRD diffraction peaks to shift to a lower 2θ angle. These results, combining the XRD patterns and the Raman results, suggest that the post-annealing treatment of the BNT-5.5BZ samples promoted the BZ component diffusion in the BNT matrix.

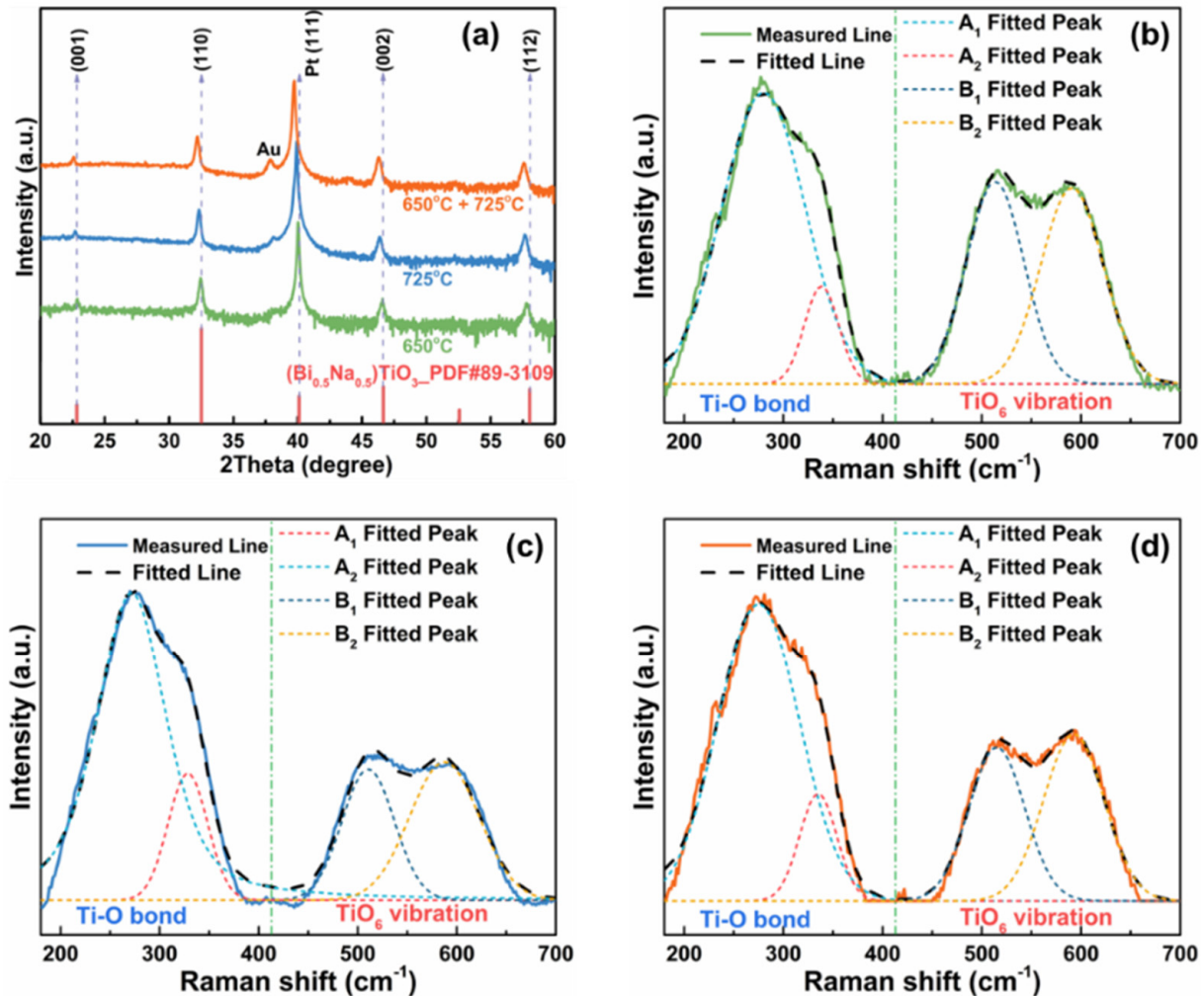


Figure 2. (a) X-ray diffraction results of the BNT-5.5BZ samples annealed under different conditions; Raman spectroscopy data with spectral deconvoluted results of the BNT-5.5BZ thin films annealed under different conditions: (b) “650 °C”, (c) “725 °C”, and (d) “650 °C + 725 °C” films.

The top-view SEM images of the BNT-5.5BZ thin films annealed in different conditions are shown in Figure 3a,c. It is obvious that the grain size of the “650 °C + 725 °C” films was larger than that of the “725 °C” films. After post-annealing, the holes decrease, and the grains grow for the BNT-5.5BZ thin films, as displayed in Figure 3c. The cross-sectional SEM images in Figure 3b,d present a dense multilayer structure consisting of the BNT-5.5BZ thin film, the bottom Pt/TiO₂ electrode, and the SiO₂/Si substrate, from the top to the bottom of the pictures. A dense columnar growth with an evident interface between the BNT-5.5BZ films and the Pt/TiO₂/SiO₂/Si (001) substrates was present in both films, as shown in Figure 3b,d. In addition, the thicknesses of the BNT-5.5BZ thin films were calculated to be 0.9 μm –1 μm from the cross-sectional SEM images. An increased grain size in the dense structure of the “650 °C + 725 °C” films annealed in the O₂ atmosphere is more beneficial to enhance the electrical properties.

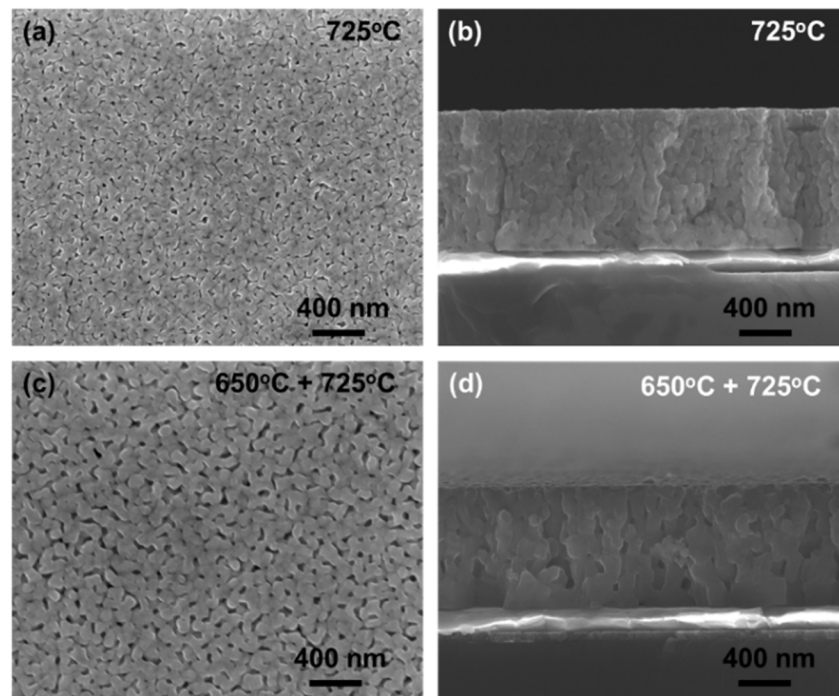


Figure 3. Surface and cross-sectional SEM images of the BNT-5.5BZ thin films annealed under different conditions: (a,b) 725 °C, and (c,d) 650 °C + 725 °C films.

Figure 4a displays the frequency dependence of the dielectric properties from 1 kHz to 1 MHz of the BNT-5.5BZ thin films. An obvious feature of frequency dispersion was exhibited by all BNT-5.5BZ samples: the dielectric constant gradually decreased, while the dielectric loss increased with the frequency increase. This phenomenon could be due to the relaxation of the dipoles, space charge polarization, and so on, similar to what observed for other BNT-based thin films [7,8]. The “650 °C + 725 °C” films showed a higher dielectric constant and a lower loss than the other samples at the same frequency from 1 kHz to 1 MHz. Furthermore, the lower dielectric loss of ~ 0.03 at 1 kHz for the “650 °C + 725 °C” thin films, is much better than those of other works reported in the literature [24,25]. The DC electric field dependence of the leakage current for the BNT-5.5BZ thin films is presented in Figure 4b. It was found that the “650 °C + 725 °C” films exhibited a lower DC leakage current at 0.4 MV/cm compared to the other films. The lower dielectric loss coincided nicely with a low leakage due to the dense and homogeneous structure of the high-quality thin films after annealing. This indicated that the post-annealing process in the O₂ atmosphere for the BNT-5.5BZ thin films likely promoted grain growth and decreased the defects inside the films.

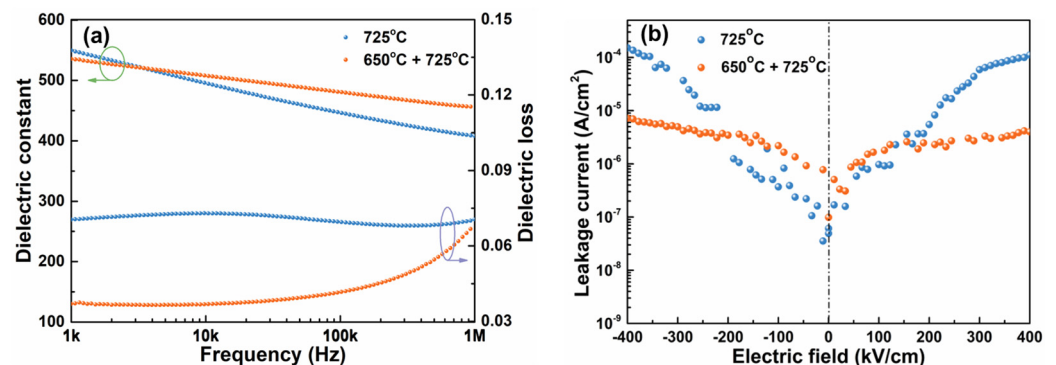


Figure 4. (a) Dielectric constant and loss as a function of frequency, (b) DC electric field dependence of the leakage current for the BNT-5.5BZ samples annealed under different conditions.

The ferroelectric hysteresis (P - E) loops at 0.9 MV/cm for the BNT-5.5BZ thin films are shown in Figure 5a. A “square-shaped” P - E loop was observed for all BNT-5.5BZ thin films, indicating a typical character of ferroelectric materials [26]. Both maximum polarization (P_{\max}) and remanent polarization (P_r) of the “725 °C” thin films were larger compared with those of the “650 °C + 725 °C” thin films. However, the P - E loop of “725 °C” thin films was not completely saturated due to a high dielectric loss and a large DC leakage current (Figure 4). It was found that the P - E loop of the “650 °C + 725 °C” thin films was slimmer and better saturated than those of other BNT-based thin films [27,28]. Figure 5b presents the dielectric constant and dielectric loss of the “650 °C + 725 °C” thin films as a function of temperature at the three different frequencies. Two dielectric anomalies of the “650 °C + 725 °C” thin films are observed in Figure 5b. The first anomaly, similar to a hump or a shoulder, was detected between 80 °C to 180 °C. An evident frequency dispersion around the characteristic temperature T_s showed a typical ferroelectric relaxor feature [8,29]. As the temperature increased, the other dielectric anomaly appeared in the temperature range of 220 °C to 300 °C. The temperature corresponding to the maximum dielectric constant is characterized as T_m . From the perspective of dielectric behavior, the “650 °C + 725 °C” thin films exhibited the coexistence of a ferroelectric phase and a relaxor state, similar to previously reported BNT-5.5BZ ceramics [19].

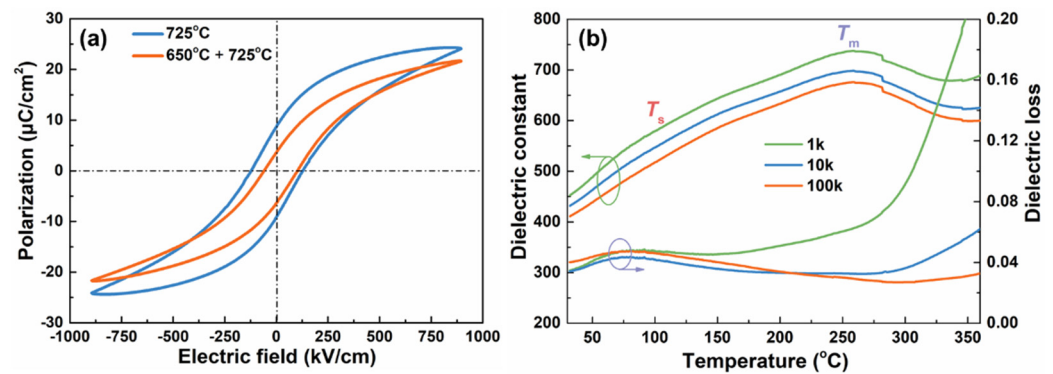


Figure 5. (a) Ferroelectric hysteresis (P - E) loops of the BNT-5.5BZ thin films annealed under different conditions and (b) dielectric constant and loss as a function of temperature for the “650 °C + 725 °C” thin films.

The bipolar and unipolar strain hysteresis (S - E) loops at 0.5 MV/cm of the BNT-5.5BZ thin films annealed under different conditions are presented in Figure 6. “Butterfly-shaped” bipolar S - E loops are observed for all BNT-5.5BZ thin films in Figure 6a, suggesting a typical ferroelectric feature. The “650 °C + 725 °C” thin films exhibited a larger bipolar strain value than the “725 °C” thin films, while the “650 °C + 725 °C” thin films showed a larger unipolar strain response, as indicated in Figure 6b. The unipolar strain of the “650 °C + 725 °C” films reached 0.63% at 0.5 MV/cm, approximately 2.2 times that of the “725 °C” thin films, i.e., 0.28%. To explore the relation of the unipolar strain response with the applied electric fields, unipolar S - E loops as a function of electric fields for the “650 °C + 725 °C” samples were determined and are displayed in Figure 6c. The unipolar strain values of the films annealed under various conditions linearly increased with the increase in the applied electric fields. It was found that an ultra-high strain response of up to 1.5% was obtained at 1.5 MV/cm for the “650 °C + 725 °C” samples, much better than those of BNT-based and non-BNT-based thin films in previous studies [30–33]. Furthermore, the withstand electric field (1.5 MV/cm, the maximum external electric field in the S - E measurement before breakdown) in the “650 °C + 725 °C” thin films was much higher than that in the “725 °C” thin films (0.5 MV/cm). A high-withstand electric field in the BNT-5.5BZ thin films after two-step annealing is helpful for device applications.

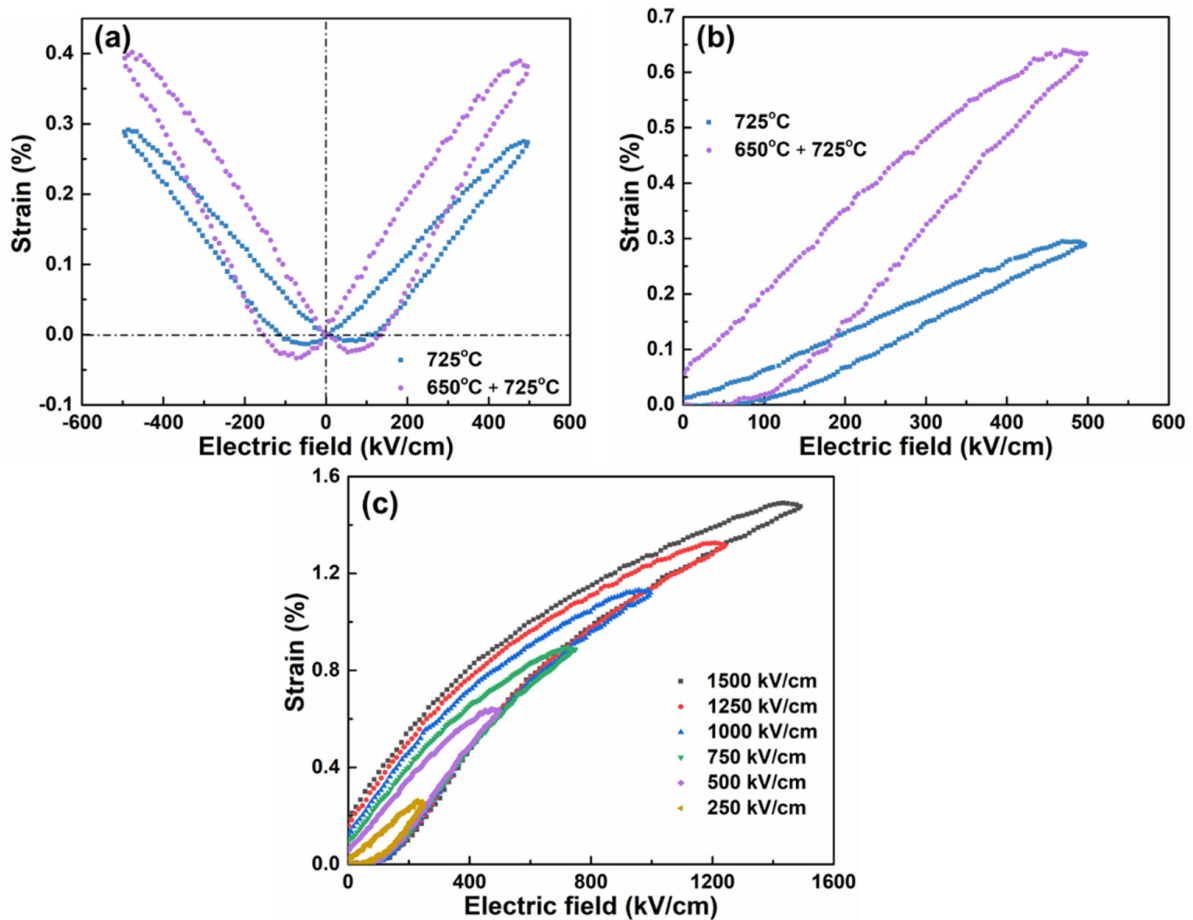


Figure 6. (a) Bipolar and (b) unipolar strain hysteresis (S - E) loops at 0.5 MV/cm for the BNT-5.5BZ thin films annealed under different conditions; (c) unipolar S - E loops as a function of the electric field for the “650 °C + 725 °C” thin films.

To further study the influence of the annealing conditions on the piezoelectric responses in different dimensions, the local polarization behavior was measured using PFM and is present in Figure 7. The out-of-plane phase-voltage and displacement-voltage hysteresis loops were determined by applying a dynamical DC bias up to 40 V superimposed on an alternating current (AC) bias ($V_{pp} = 5000$ mV, $f = 280$ kHz) on the film surface via the PFM tips. Many researchers have confirmed that the piezoelectric response detected using the PFM method is highly dependent on the PFM measurement conditions, such as laser location, measuring parameters, tip types, tiny contact area, and so on [7,8]. Therefore, all BNT-5.5BZ thin films were measured under the same conditions in this work. “Square-shaped” phase hysteresis loops (in Figure 7a,b) were shown for all BNT-5.5BZ thin films, demonstrating a typical characteristic of the piezoelectric behavior. Figure 7c,d shows “butterfly-like” displacement loops measured inside an individual grain in all BNT-5.5BZ thin films. The “650 °C + 725 °C” thin films exhibited a more significant displacement value than the “725 °C” thin films, possibly attributed to the crystal lattice extension and distortion inside the individual grains. Furthermore, a pronounced asymmetry can be seen in both phase-voltage and displacement-voltage butterfly hysteresis loops, mainly caused by the built-in electric field and determined by charges and defects during the poling process [27]. In addition, the unsymmetrical configuration of the different types of Au top and Pt bottom electrodes in the films cannot be neglected. As a result, a higher micro-scale piezoelectric response was obtained in the films after annealing.

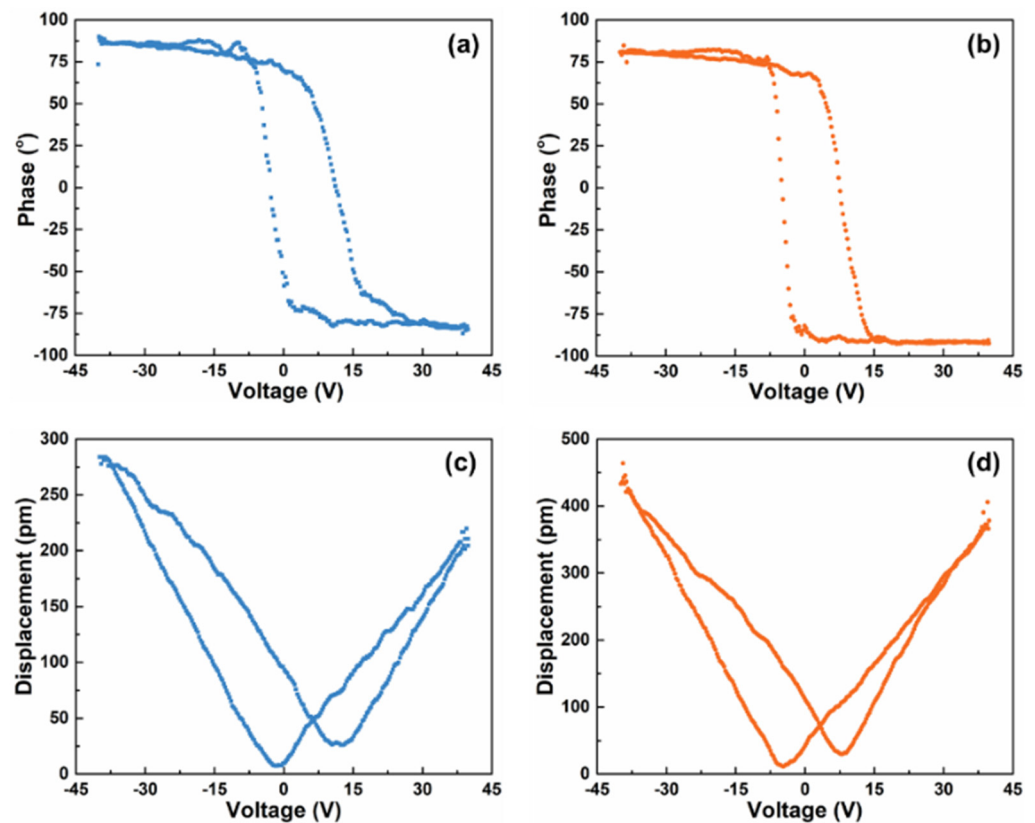


Figure 7. Out-of-plane phase–voltage and displacement–voltage butterfly hysteresis loops of the BNT–5.5BZ thin films annealed under different conditions: (a,c) “725 °C”, and (b,d) “650 °C + 725 °C” films.

After annealing, an enhanced unipolar strain of $\sim 1.5\%$ and a reduced dielectric loss of ~ 0.03 were exhibited in the BNT–5.5BZ thin films. It indicated that the post-annealing treatment in the O_2 atmosphere played an essential role in improving the strain responses for the BNT–5.5BZ thin films. A primary crystallization was present in the samples annealing at 650 °C, as shown by the XRD and Raman results. However, when post-annealed at 725 °C in an O_2 atmosphere, the films might exhibit a complete crystallization with a large grain size. For BNT-based ceramics, the strain response strongly depends on the grain size. The strain response can be improved by increasing the grain size for ceramics with a dense structure [34]. The grain size growth in the BNT–5.5BZ films after the annealing treatment made it possible to achieve a much larger micro-scale polarization response (Figure 7) compared to the non-annealed samples. Post-annealing treatments are commonly used to reduce the oxygen vacancies and release residual stresses both on surfaces and inside films [35]. Furthermore, oxygen interacts with oxygen vacancies in the films, increasing the grain size when annealing the films at high temperatures in an O_2 atmosphere [17]. In this work, the post-annealing in an O_2 atmosphere for the BNT–5.5BZ thin films could effectively decrease defects due to the volatility of alkali metal elements during the heating process. The appearance of oxygen vacancies could be inhibited in this process, and an improvement of the grain size was achieved, as shown in the top-view microstructure due to the increased annealing time [36]. The BNT–5.5BZ thin films presented the coexistence of the ferroelectric phase and the relaxor state, as shown by their dielectric behaviors under different temperatures in Figure 5b. As studied in our previous works [8,37], a significant strain response is easier to realize near the ferroelectric and relaxor phase boundary thanks to a reversible field-induced phase transition [38]. Therefore, post-annealing in an O_2 atmosphere effectively optimized the quality and strain responses of the BNT-based thin films.

4. Conclusions

In this work, a two-step annealing treatment optimized the quality and strain response of BNT-5.5BZ thin films deposited on Pt/TiO₂/SiO₂/Si (001) substrates by the CSD method. It was revealed that the annealing method significantly affected the morphology and electrical performances of the BNT-5.5BZ thin films. The BNT-5.5BZ thin films, after annealing at 725 °C in an O₂ atmosphere, showed excellent properties: a homogeneous and dense structure, an enhanced strain response of ~ 1.5%, and a lower dielectric loss of ~0.03 at RT and a frequency of 1 kHz. These properties were much better than those of the films without post-annealing treatment. These results indicate that BNT-5.5BZ thin films with an excellent strain response provide more possibilities for minimized applications such as micro-actuators.

Author Contributions: Conceptualization, J.Z. and W.R.; methodology, J.Z. and Z.W.; validation, W.R.; formal analysis, J.Z. and Z.W.; investigation, Z.W.; data curation, J.Z. and Z.W.; writing—original draft preparation, Z.W.; writing—review and editing, J.Z. and W.R.; supervision, J.Z. and W.R.; project administration, J.Z. and W.R.; funding acquisition, J.Z. and W.R. All authors have read and agreed to the published version of the manuscript.

Funding: This work was supported by the Natural Science Foundation of China (Grant No. 51902246), the China National Key R&D Program (Grant No. 2021YFB3201800 and 2020YFC0122100), the Fundamental Research Funds for the Central Universities (xzd012020059), the “111 Project” of China (B14040), the Xijiang Innovation Team Introduction Program of Zhaoqing (Jiecheng).

Data Availability Statement: Not applicable.

Acknowledgments: We acknowledge the Instrument Analysis Center of Xi’an Jiaotong University for the assistance with Raman analysis. We acknowledge the Instrument Analysis Center of Xi’an Jiaotong University for the assistance with SEM measurements.

Conflicts of Interest: The authors declare no conflict of interest.

References

1. Trolier-McKinstry, S.; Zhang, S.J.; Bell, A.J.; Tan, X.L. High-Performance Piezoelectric Crystals, Ceramics, and Films. *Annu. Rev. Mater. Res.* **2018**, *48*, 191–217. [[CrossRef](#)]
2. Ali, W.R.; Prasad, M. Piezoelectric MEMS based acoustic sensors: A review. *Sens. Actuators A Phys.* **2020**, *301*, 111756. [[CrossRef](#)]
3. Martin, L.W.; Rappe, A.M. Thin-film ferroelectric materials and their applications. *Nat. Rev. Mater.* **2017**, *2*, 16087. [[CrossRef](#)]
4. Fan, P.Y.; Liu, K.; Ma, W.G.; Tan, H.; Zhang, Q.; Zhang, L.; Zhou, C.R.; Salamon, D.; Zhang, S.-T.; Zhang, Y.J.; et al. Progress and perspective of high strain NBT-based lead-free piezoceramics and multilayer actuators. *J. Mater.* **2021**, *7*, 508–544. [[CrossRef](#)]
5. Zhang, S.-T.; Kouna, A.B.; Aulbach, E.; Ehrenberg, H.; Rödel, J. Giant strain in lead-free piezoceramics Bi_{0.5}Na_{0.5}TiO₃-BaTiO₃-K_{0.5}Na_{0.5}NbO₃ system. *Appl. Phys. Lett.* **2007**, *91*, 112906. [[CrossRef](#)]
6. Liu, X.M.; Tan, X.L. Giant strains in non-textured (Bi_{1/2}Na_{1/2})TiO₃-based lead-free ceramics. *Adv. Mater.* **2016**, *28*, 574–578. [[CrossRef](#)]
7. Zhao, J.Y.; Niu, G.; Ren, W.; Wang, L.Y.; Zhang, N.; Sun, Y.X.; Wang, Q.; Shi, P.; Liu, M.; Zhao, Y.L. Polarization behavior of lead-free 0.94(Bi_{0.5}Na_{0.5})TiO₃-0.06BaTiO₃ thin films with enhanced ferroelectric properties. *J. Eur. Ceram. Soc.* **2020**, *40*, 3928–3935. [[CrossRef](#)]
8. Wang, Z.; Zhao, J.Y.; Niu, G.; Ren, W.; Zhang, N.; Zheng, K.; Quan, Y.; Wang, L.Y.; Zhuang, J.; Cai, H.H.; et al. Giant strain responses and relaxor characteristics in lead-free (Bi_{0.5}Na_{0.5})TiO₃-BaZrO₃ ferroelectric thin films. *J. Mater. Chem. C* **2022**, *10*, 7449–7459. [[CrossRef](#)]
9. Zhu, K.; Wu, S.H.; Song, B.J.; Ge, G.L.; Shi, Y.J.; Xu, L.X.; Yan, H.; Shen, B.; Zhai, J.W. Multi-domain BNiT modification enhanced the piezoelectric properties of BNT-based lead-free thin films. *J. Mater. Chem. C* **2020**, *8*, 17114–17121. [[CrossRef](#)]
10. Ni, F.E.; Zhu, K.; Xu, L.X.; Liu, Y.; Yan, H.; Shen, B.; Zhai, J.W. Piezoelectric enhancement and vacancy defect reduction of lead-free Bi_{0.5}Na_{0.5}TiO₃-based thin films. *Ceram. Int.* **2022**, *48*, 12601–12607. [[CrossRef](#)]
11. Xu, L.X.; Wu, S.H.; Zhu, K.; Song, B.J.; Zhou, X.F.; Yan, H.; Shen, B.; Zhai, J.W. Enhanced piezoelectricity and reduced leakage current of a novel (1-x)Bi_{0.5}Na_{0.5}TiO₃-x(Sr_{0.7}Bi_{0.2}□_{0.1})TiO₃ thin film. *Inorg. Chem. Front.* **2021**, *8*, 700–710. [[CrossRef](#)]
12. Alonso-Sanjósé, D.; Jiménez, R.; Bretos, I.; Calzada, M.L. Lead-free ferroelectric (Na_{1/2}Bi_{1/2})TiO₃-BaTiO₃ thin films in the morphotropic phase boundary composition: Solution processing and properties. *J. Am. Ceram. Soc.* **2009**, *92*, 2218–2225. [[CrossRef](#)]
13. Zhao, H.F.; Liu, X.S.; Ren, W.; Zhang, Y.J. Preparation and characterization of lead zirconate titanate thin films grown by RF magnetron sputtering for pyroelectric infrared detector arrays. *Ceram. Int.* **2018**, *44*, S7–S10. [[CrossRef](#)]

14. Weng, C.-M.; Tsai, C.-C.; Hong, C.-S.; Lin, C.-C.; Chen, C.-C.; Chu, S.-Y.; Sheen, J.; Chen, Z.-Y.; Su, H.-H. Effects of non-stoichiometry on the microstructure, oxygen vacancies, and electrical properties of KNN-based thin films. *ECS J. Solid State Sci. Technol.* **2016**, *5*, N49–N56. [[CrossRef](#)]
15. Huang, J.-H.; Wong, M.-S. Structures and properties of titania thin films annealed under different atmosphere. *Thin Solid Film.* **2011**, *520*, 1379–1384. [[CrossRef](#)]
16. Bursill, L.A.; Brooks, K.G. Crystallization of sol-gel derived lead-zirconate-titanate thin films in argon and oxygen atmospheres. *J. Appl. Phys.* **1994**, *75*, 4501–4509. [[CrossRef](#)]
17. Bulyarskiy, S.V.; Koiva, D.A.; Gusarov, G.G.; Latipov, E.V.; Rudakov, G.A.; Svetukhin, V.V. Crystallization of amorphous titanium oxide films upon annealing in an oxygen atmosphere. *Mater. Sci. Eng. B* **2022**, *283*, 115802. [[CrossRef](#)]
18. Reddy, S.R.; Prasad, V.V.B.; Bysakh, S.; Shanker, V.; Hebalkar, N.; Roy, S.K. Superior energy storage performance and fatigue resistance in ferroelectric BCZT thin films grown in an oxygen-rich atmosphere. *J. Mater. Chem. C* **2019**, *7*, 7073–7082. [[CrossRef](#)]
19. Rahman, J.U.; Hussain, A.; Maqbool, A.; Song, T.K.; Kim, W.J.; Kim, S.S.; Kim, M.H. Dielectric, ferroelectric and field-induced strain response of lead-free BaZrO₃-modified Bi_{0.5}Na_{0.5}TiO₃ ceramics. *Curr. Appl. Phys.* **2014**, *14*, 331–336. [[CrossRef](#)]
20. Kunej, Š.; Veber, A.; Suvorov, D.; Randall, C. Sol-gel synthesis and characterization of Na_{0.5}Bi_{0.5}TiO₃-NaTaO₃ thin films. *J. Am. Ceram. Soc.* **2013**, *96*, 442–446. [[CrossRef](#)]
21. Aksel, E.; Forrester, J.S.; Kowalski, B.; Deluca, M.; Damjanovic, D.; Jones, J.L. Structure and properties of Fe-modified Na_{0.5}Bi_{0.5}TiO₃ at ambient and elevated temperature. *Phys. Rev. B* **2012**, *85*, 204121. [[CrossRef](#)]
22. Hao, J.G.; Xu, Z.J.; Chu, R.Q.; Li, W.; Fu, P.; Du, J.; Li, G.R. Structure evolution and electrostrictive properties in (Bi_{0.5}Na_{0.5})_{0.94}Ba_{0.06}TiO₃-M₂O₅ (M = Nb, Ta, Sb) lead-free piezoceramics. *J. Eur. Ceram. Soc.* **2016**, *36*, 4003–4014. [[CrossRef](#)]
23. Zhao, J.Y.; Zhang, N.; Quan, Y.; Niu, G.; Ren, W.; Wang, Z.; Zheng, K.; Zhao, Y.L.; Ye, Z.-G. Evolution of mesoscopic domain structure and macroscopic properties in lead-free Bi_{0.5}Na_{0.5}TiO₃-BaTiO₃ ferroelectric ceramics. *J. Appl. Phys.* **2021**, *129*, 084103. [[CrossRef](#)]
24. Sun, N.N.; Li, Y.; Zhang, Q.W.; Hao, X.H. Giant energy-storage density and high efficiency achieved in (Bi_{0.5}Na_{0.5})TiO₃-Bi(Ni_{0.5}Zr_{0.5})O₃ thick films with polar nanoregions. *J. Mater. Chem. C* **2018**, *6*, 10693–10703. [[CrossRef](#)]
25. Wu, S.H.; Song, B.J.; Li, P.; Chen, P.; Shen, B.; Zhai, J.W. Reduced leakage current and enhanced piezoelectricity of BNT-BT-BMO thin films. *J. Am. Ceram. Soc.* **2019**, *103*, 1219–1229. [[CrossRef](#)]
26. Zhou, Z.; Luo, J.; Sun, W.; Li, J.-F. Temperature and composition dependent phase transitions of lead-free piezoelectric (Bi_{0.5}Na_{0.5})TiO₃-BaTiO₃ thin films. *Phys. Chem. Chem. Phys.* **2017**, *19*, 19992–19997. [[CrossRef](#)]
27. Zhou, Z.; Sun, W.; Li, J.-F. Sol-gel synthesis of 0.94(Bi_{0.5}Na_{0.5})TiO₃-0.06BaTiO₃ lead-free piezoelectric films: Effect of pyrolysis temperature on phase evolution and electrical properties. *J. Sol-Gel Sci. Technol.* **2016**, *77*, 423–429. [[CrossRef](#)]
28. Fan, P.Y.; Zhang, Y.Y.; Huang, J.Q.; Hu, W.; Huang, D.; Liu, Z.P.; Xie, B.; Li, X.D.; Xiao, J.Z.; Zhang, H.B. Constrained sintering and electrical properties of BNT-BKT lead-free piezoceramic thick films. *Ceram. Int.* **2016**, *42*, 2534–2541. [[CrossRef](#)]
29. Jing, R.Y.; Zhang, L.Y.; Hu, Q.Y.; Alikin, D.O.; Shur, V.Y.; Wei, X.Y.; Zhang, L.; Liu, G.; Zhang, H.B.; Jin, L. Phase evolution and relaxor to ferroelectric phase transition boosting ultrahigh electrostrains in (1-x)(Bi_{1/2}Na_{1/2})TiO₃-x(Bi_{1/2}K_{1/2})TiO₃ solid solutions. *J. Mater.* **2021**, *8*, 335–346. [[CrossRef](#)]
30. Liu, H.J.; Wu, H.J.; Ong, K.P.; Yang, T.N.; Yang, P.; Das, P.K.; Chi, X.; Zhang, Y.; Diao, C.Z.; Wong, W.K.A.; et al. Giant piezoelectricity in oxide thin films with nanopillar structure. *Science* **2020**, *369*, 292–297. [[CrossRef](#)]
31. Cai, H.H.; Yan, S.G.; Zhou, M.X.; Liu, N.T.; Ye, J.M.; Li, S.; Cao, F.; Dong, X.L.; Wang, G.S. Significantly improved energy storage properties and cycling stability in Ladoped PbZrO₃ antiferroelectric thin films by chemical pressure tailoring. *J. Eur. Ceram. Soc.* **2019**, *39*, 4761–4769. [[CrossRef](#)]
32. Wang, L.Y.; Ren, W.; Ma, W.H.; Liu, M.; Shi, P.; Wu, X.Q. Improved electrical properties for Mn-doped lead-free piezoelectric potassium sodium niobate ceramics. *AIP Adv.* **2015**, *5*, 097120. [[CrossRef](#)]
33. Wang, L.Y.; Ren, W.; Yao, K.; Goh, P.C.; Shi, P.; Wu, X.Q.; Yao, X. Effect of pyrolysis temperature on K_{0.5}Na_{0.5}NbO₃ thick films derived from polyvinylpyrrolidone-modified chemical solution. *J. Am. Ceram. Soc.* **2010**, *93*, 3686–3690. [[CrossRef](#)]
34. Li, H.-L.; Liu, Q.; Zhou, J.-J.; Wang, K.; Li, J.-F.; Liu, H.; Fang, J.-Z. Grain size dependent electrostrain in Bi_{1/2}Na_{1/2}TiO₃-SrTiO₃ incipient piezoceramics. *J. Eur. Ceram. Soc.* **2016**, *36*, 2849–2853. [[CrossRef](#)]
35. Kim, M.-K.; Ji, S.-Y.; Lim, J.-H.; Kim, S.-W.; Jeong, D.-Y. Energy storage performance and thermal stability of BNT-SBT with artificially modulated nano-grains via aerosol deposition method. *J. Asian Ceram. Soc.* **2022**, *10*, 196–202. [[CrossRef](#)]
36. Sakamoto, W.; Makino, N.; Lee, B.-Y.; Iijima, T.; Moriya, M.; Yogo, T. Influence of volatile element composition and Mn doping on the electrical properties of lead-free piezoelectric (Bi_{0.5}Na_{0.5})TiO₃ thin films. *Sens. Actuators A Phys.* **2013**, *200*, 60–67. [[CrossRef](#)]
37. Wang, Z.; Zhao, J.Y.; Zhang, N.; Ren, W.; Zheng, K.; Quan, Y.; Zhuang, J.; Zhang, Y.J.; Jiang, L.Y.; Wang, L.Y.; et al. Optimizing strain response in lead-free (Bi_{0.5}Na_{0.5})TiO₃-BaTiO₃-NaNbO₃ solid solutions via ferroelectric/(non-)ergodic relaxor phase boundary engineering. *J. Mater.* **2022**, *9*, 244–255. [[CrossRef](#)]
38. Zhou, X.F.; Yang, H.P.; Xue, G.L.; Luo, H.; Zhang, D. Optimized strain performance in <001>-textured Bi_{0.5}Na_{0.5}TiO₃-based ceramics with ergodic relaxor state and core-shell microstructure. *J. Adv. Ceram.* **2022**, *11*, 1542–1558.

Disclaimer/Publisher’s Note: The statements, opinions and data contained in all publications are solely those of the individual author(s) and contributor(s) and not of MDPI and/or the editor(s). MDPI and/or the editor(s) disclaim responsibility for any injury to people or property resulting from any ideas, methods, instructions or products referred to in the content.